2D mutually synchronised spin Hall nano-oscillator arrays for neuromorphic computing

Mohammad Zahedinejad[1,2,*], Ahmad A. Awad[1,2,*], Shreyas Muralidhar[1,*], Roman Khymyn[1,2], Himanshu Fulara[1,2], Hamid Mazraati[2,3], Mykola Dvornik[1,2], and Johan Åkerman[1,2,3]

[1] *Physics Department, University of Gothenburg, 412 96 Gothenburg, Sweden*

[2] *NanOsc AB, Electrum 229, 164 40 Kista, Sweden*

[3] *Material and Nanophysics, School of Engineering Sciences, KTH Royal Institute of Technology, Electrum 229, 164 40 Kista, Sweden*

[*] *These authors contributed equally to this work.*

Spin Hall nano-oscillators (SHNOs) utilize pure spin currents to drive local regions of magnetic films and nanostructures into auto-oscillating precession. If such regions are placed in close proximity to each other they can interact and may mutually synchronise.Here we demonstrate robust mutual synchronisation of two-dimensional SHNO arrays ranging from 2×2 to 8×8 nano-constrictions, observed both electrically and using micro-Brillouin Light Scattering microscopy. On short time-scales, where the auto–oscillation linewidth is governed by white noise, the signal quality factor, $Q = f/\Delta f$, increases linearly with number of mutually synchronised nano-constrictions (N), reaching 170,000 in the largest arrays. We also show that SHNO arrays exposed to two independently tuned microwave frequencies exhibit the same synchronisation maps as can be used for neuromorphic vowel recognition. Our demonstrations may hence enable the use of SHNO arrays in two-dimensional oscil-

lator networks for high-quality microwave signal generation and ultra-fast neuromorphic computing.

Interest in bio-inspired oscillatory computing[1–3] is rapidly increasing in an effort to mitigate the inevitable end of Moore's law.[4] Although neuronal activities may seem slow, our brain is the most energy efficient processing device for cognitive tasks thanks to its massively interconnected oscillatory neurons[5]. While recent memristive[6,7], superconducting[8,9], optical[10,11], and micromechanical[12,13] oscillator arrays have been demonstrated, realizing a large physical oscillatory network that meets technical requirements such as room temperature operation, scaling, integration, high speed, and low power consumption remains a challenge.

Spin transfer torque nano-oscillators (STNOs) are one of the most promising candidates addressing these requirements.[14–16] Free running STNOs can interact electrically and/or magnetically and mutually synchronise to deliver higher power and more coherent microwave signals with quality factors as high as Q = 18,000 [17]. A recent study demonstrated vowel recognition using reservoir computing on four electrically synchronised STNOs[18] achieving a performance comparable to state-of-the-art CMOS. However, to process more complicated tasks, large arrays of mutually synchronised oscillators are needed.

Spin Hall nano-osillators[19,20] (SHNOs) have recently emerged as an attractive alternative as they can be fabricated more easily and directly onto silicon substrates[21]. As with STNOs, this makes them compatible with both back and front end of lines in CMOS technology. Their magnetisation dynamics is driven by pure spin currents generated by charge currents in a heavy metal layer with a strong spin Hall effect.[22–24] The spin current can exert negative damping on an adjacent ferromagnetic layer and eventually overcome the intrinsic damping, resulting in a steady precession of the magnetisation around the effective magnetic field.[19]

Nano-constriction SHNOs can be fabricated in chains where they can show mutual synchronisation of up to nine individual constrictions.[25] Here we demonstrate that nano-constriction SHNOs can also be mutually synchronised in two-dimensional arrays comprised of as many as 64 SHNOs. Each oscillator (neuron) within the 2D array interacts with its nearest neighbors via both exchange and dipolar coupling, which can be tuned by both the drive current and the strength and direction of the magnetic field. As expected from theory[26], the signal quality factor of the mutually synchronised state increases linearly with the number of synchronised SHNOs, reaching Q = 170,000 for 64 SHNOs. We also demonstrate that these arrays lend themselves as-is to neuromorphic computing of the type recently employed for vowel recognition.[18] Adding two microwave currents with different frequencies to the drive current of a 4x4 SHNO array, we demonstrate the emergence of 20 different injection locked states depending on the input combination of the two frequencies.

Schematic of SHNO array and device layout

Fig.1 shows the schematic of an SHNO array with the oscillators illustrated by green arrows precessing around the effective magnetic field (H). The out-of-plane (θ) and in-plane (ϕ) angles of H are indicated in the coordinate system while the charge current direction is shown by a blue arrow. The Pt, Hf, and NiFe layers are shown with their thicknesses in nm and highlighted by blue, red and gray colors, respectively. The ultra-thin Hf layer reduces the spin memory loss at the Pt/NiFe interface[27], which decreases the damping and hence the threshold current. The lower left inset shows the microwave co-planar waveguide (CPW) used for electrical measurements with the location of the SHNO array indicated by a black rectangle (see Methods for Sample fabrication details).

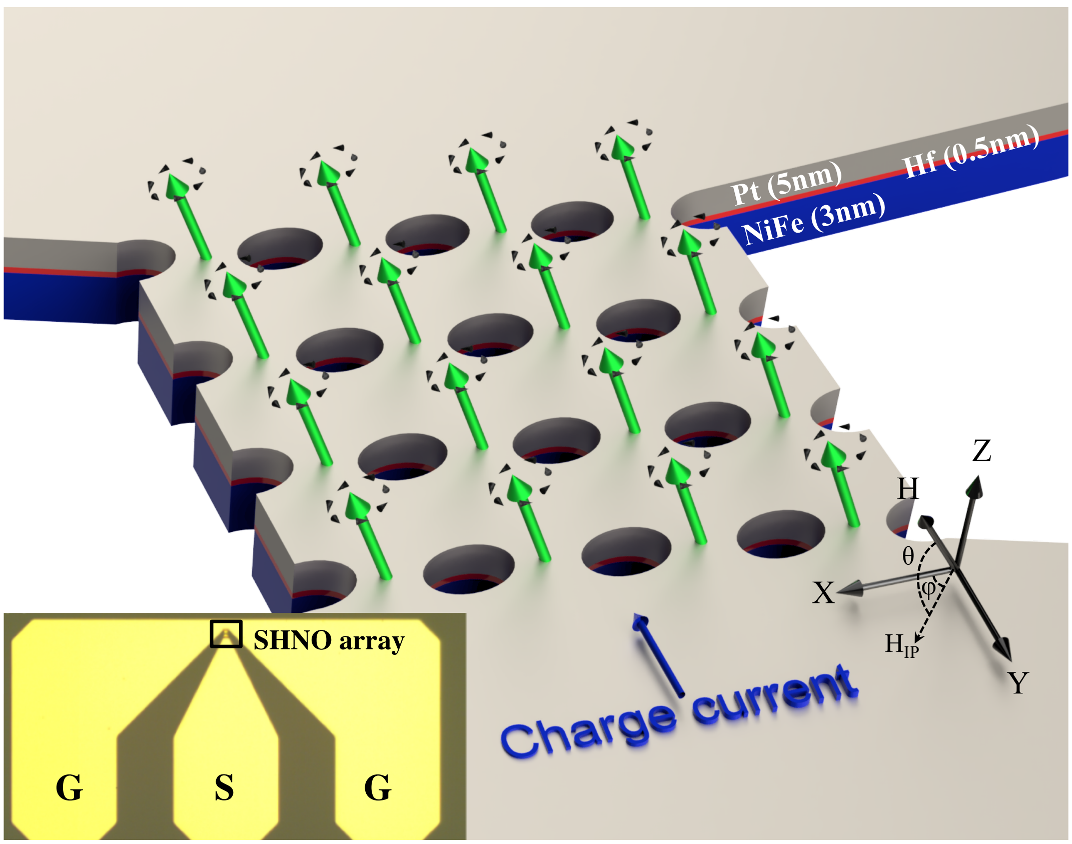

Figure 1: **Schematic representation of a 4×4 SHNO array.** The schematic shows the direction of the applied magnetic field (H), its in-plane component (H_{IP}), and the charge current. The green arrows indicate the precessing magnetisation of each nano-constriction. The Pt, Hf, and NiFe layers are highlighted by gray, red, and blue colors with corresponding thicknesses in nm. The inset shows an optical microscopy image of the ground-signal-ground co-planar wave guide used for electrical measurements.

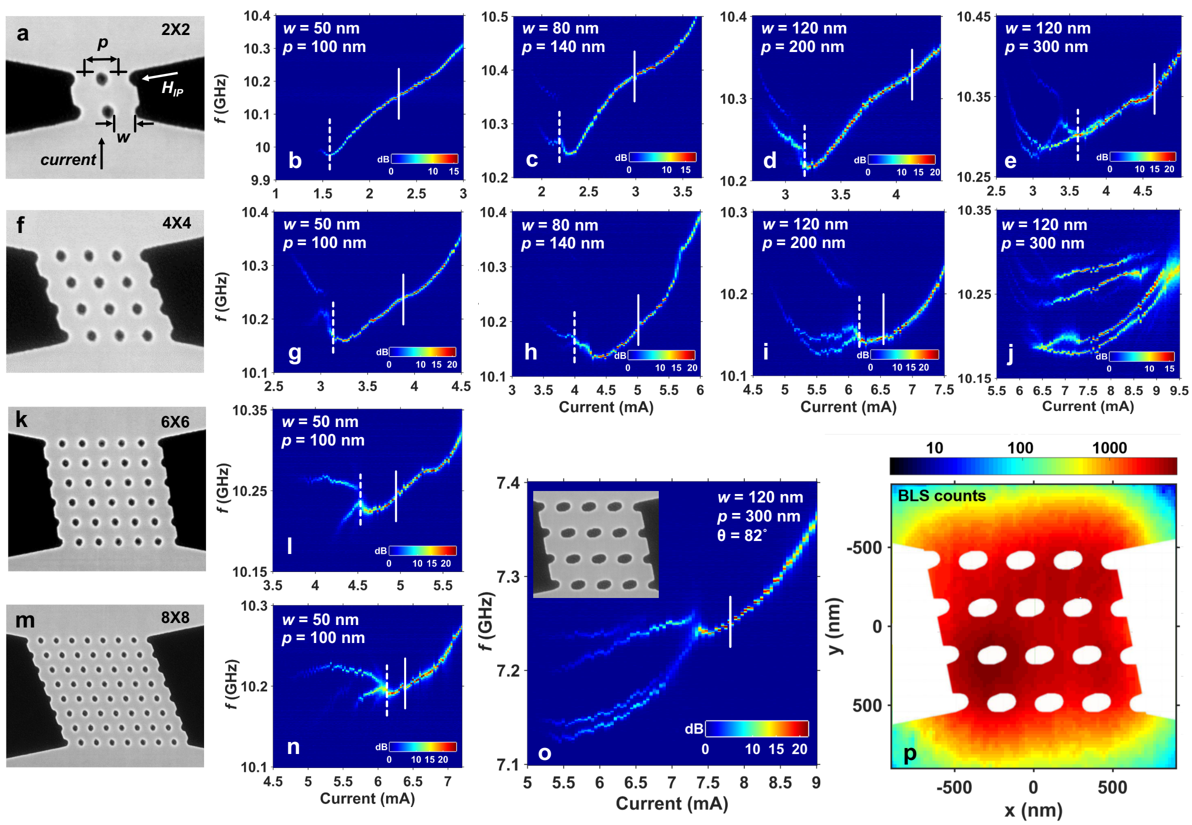

Figure 2: **Power spectral density and micro-Brillouin Light Scattering microscopy of spin Hall nano-oscillator arrays.** All data was acquired in a magnetic field of 0.68 T with an out-of-plane angle of 76° and an in-plane angle of 30°. All PSD scale bars are shown in dB over noise floor(**a**) SEM image of a 2x2 SHNO array showing the definition of the width (w) and the pitch (p). The direction of the charge current is shown by a solid black while the in-plane angle of applied magnetic field (H_{IP}) is presented by a white solid arrow. (**b** to **e**) PSD of four different 2x2 SHNO arrays with different constriction widths (50, 80, and 120 nm) and SHNOs center to center distance as pitch size (100, 140, 200, 300 nm). White dashed lines indicate the current at which the SHNO within the arrays come to a synchronised state (**f**) SEM picture of a 4x4 SHNO array. (**g** to **j**) PSD of four different 4x4 arrays having the same width and pitch as the 2x2 arrays in **b** to **e**. Mutual synchronisation is only observed in the first three SHNO arrays. (**k**) and (**m**) SEM pictures of a 6x6 and an 8x8 SHNO array. (**l**) and (**n**) PSD of the 6x6 and the 8x8 SHNO arrays with the smallest w and p, both showing robust mutual synchronisation. (**o**) PSD of the same 4x4 array as in **j** with the out-of-plane field angle increased from 76° to 82° to increase the coupling between SHNOs. The inset shows the SEM image of the defined array. (**p**) Micro-Brillouin Light Scattering microscopy image of the 4x4 array in **o** obtained at an operating point of I = 7.6 mA (white dashed line) showing that the entire array contributes to the spin wave excitations in the synchronised state; BLS counts are shown on a logarithmic scale.

Mutual synchronisation of SHNO arrays

We fabricated 24 different square SHNO arrays with number of nano-constrictions varied from 2×2 to 10×10 and w and p chosen as (w, p) = $(50, 100)$, $(80, 140)$, $(120, 200)$, and $(120, 300)$, where w defines the constriction width, and p stands for pitch (*i.e.* nano-constriction center to center distance; all numbers in nanometers). Fig.2a shows an SEM image of a 2×2 array with the design parameters w and p defined. Fig.2f, Fig.2k, and Fig.2m in the same column show the corresponding SEM images for a 4×4, 6×6, and 8×8 array with $(w$,$p)$= $(120, 200)$ (see Methods). The array has a slight tilt angle to better accommodate for the 30° in-plane angle of the applied field, since the auto-oscillating regions extend outwards in a direction perpendicular to this angle.

Fig.2b-e show the power spectral density (PSD) for the four different 2×2 arrays as a function of total drive current through the array. All PSDs show the typical non-monotonic current dependent frequency as the nano-constriction edge mode expands with current.[25,28] All four arrays exhibit mutual synchronisation at a synchronisation current which increases linearly with w.

Fig.2g-j show the corresponding PSD vs. current for the four different 4×4 arrays. While the overall non-monotonic current dependence of the frequency is approximately the same as in the 2×2 arrays, mutual synchronisation is now only achieved in the three first arrays. The 4×4 arrays with 300 nm separation instead show four distinct individual signals, all with approximately the same linewidth and peak power, indicating partial mutual synchronisation. BLS scans along the chains and rows of this state reveal that the chains synchronise before the rows (see Extended Data Figure 1 for details). The coupling strength is hence stronger along the chains than in between chains. The behavior of the 5×5 array is essentially identical with the 4×4 array: complete synchronisation in the first two arrays, partial synchronisation at 200 nm and 300 nm separation (see Supplementary Fig.1).

Fig.2l&n show the PSD of the 6×6 and 8×8 arrays at the smallest dimensions. At all larger dimensions, neither the 6×6 nor the 8×8 array showed complete mutual synchronisation (see Supplementary Fig.1). Similarly, the 10×10 arrays did not show complete mutual synchronisation at any dimension.

The auto-oscillating regions can be expanded by increasing the out-of-plane field angle,[28] which should increase the coupling and allow us to synchronise larger arrays. Fig.2o shows a 4×4 array similar to the one in Fig.2j but measured at an increased field angle of 82°. The four signals from the individually synchronised chains now merge into a single signal at about 7.3 mA, confirming the important role of the out-of-plane field angle to control the coupling strength. At a separation of 300 nm it then becomes meaningful to explore the spatial profile of the synchronised state using micro–Brillouin Light Scattering microscopy ($\sim$300 nm resolution), as the separation is large enough for variations within the array to be resolved. Fig.2p shows that the entire 4×4 array is energized with a relatively uniform spin wave intensity throughout the array (see Methods for Micro–BLS characterisation).

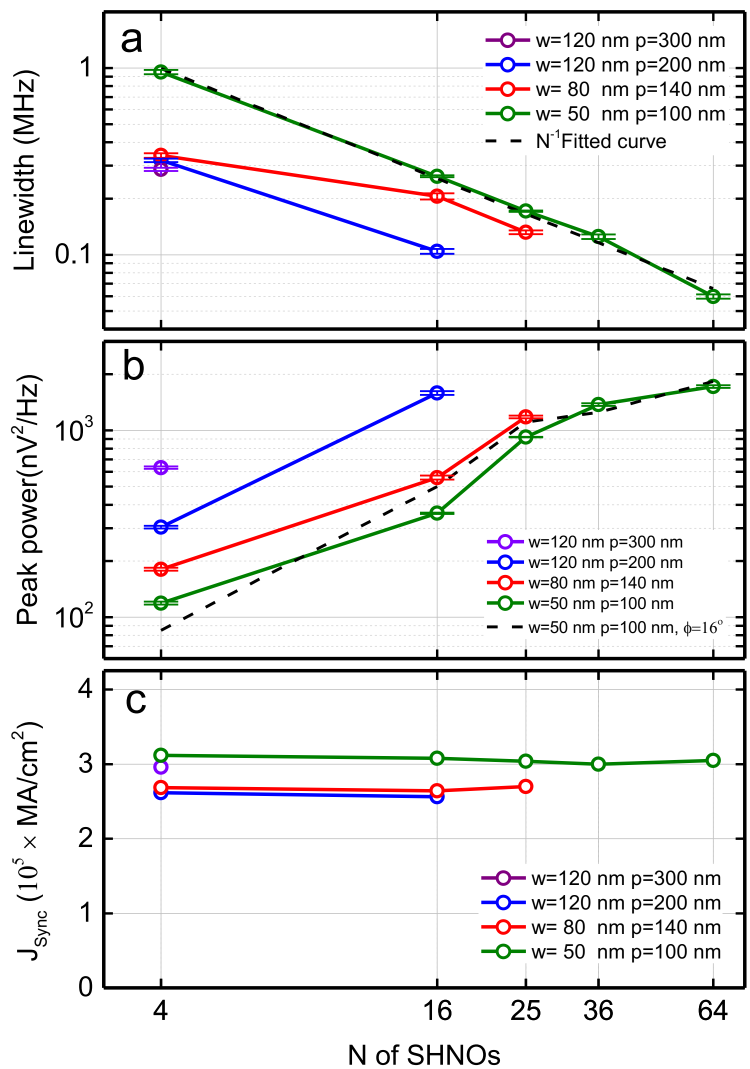
a
b
c
w=120 nm p=300 nm
w=120 nm p=200 nm
w= 80 nm p=140 nm
w= 50 nm p=100 nm
N-1 Fitted curve
w=120 nm p=300 nm
w=120 nm p=200 nm
w=80 nm p=140 nm
w=50 nm p=100 nm
w=50 nm p=100 nm, ϕ=16°
w=120 nm p=300 nm
w=120 nm p=200 nm
w= 80 nm p=140 nm
w= 50 nm p=100 nm
Linewidth (MHz)
Peak power(nV2/Hz)
JSync (105 × MA/cm2)
N of SHNOs
4
16
25
36
64

107

Figure 3: **Linewidth, peak power and synchronisation current density analysis of SHNO arrays.** (**a**) Linewidth of arrays of different w and p plotted for those array which reach robust synchronisation at operating currents indicated by white solid lines in Fig.2. Black dashed line shows predicted linewidth scaling of $\Delta f \propto N^{-1}$. (**b**) Peak power values measured for all synchronised points shown in a. Black dashed line indicates the analytical calculation of peak power for arrays with (w,p)= $(50, 100)$ considering the phase difference. The error bars (horizontal double lines) in (a) and (b) were obtained from Lorentzian fits to the experimental data. (**c**) synchronisation current density for arrays with different (w,p).

Linewidth and peak power analysis

In Fig.3 we summarize the microwave signal properties of all arrays showing complete mutual synchronisation. The linewidth plotted in Fig.3a was chosen as the lowest value observed at certain operating currents (indicated by white solid lines in Fig.2) in the mutually synchronised regions for ten consecutive measurements for arrays of different size. We found this approach to yield consistent values and a consistent trend between arrays since the frequency showed a tendency to sometimes jump over a much wider range (see Supplementary Fig.2 and 3). When comparing the individual spectrum analyzer measurements most of them would yield the same narrow linewidth, albeit at different central frequencies, but sometimes the measurement would be artificially broad due to the slower movement of the central frequency. This behavior suggests two different types of noise: *i*) a frequency independent white noise at short time scales, and *ii*) a $1/f$-like noise at longer time scales; both noise types are well established in STNOs [29].

The black dashed line in Fig.3a is a fit to N^{-1}, which clearly shows how the linewidth in the white noise regime decreases in inverse proportion to the number of mutually synchronised constrictions. This is consistent with the total mode volume, or total energy of the auto-oscillation state, increasing linearly with N.[26] As the mode volume scales with w, the linewidth is further reduced in large constrictions. As shown in the see Supplementary Fig.4, the $1/f$ noise scales more weakly than N^{-1} and only shows marginal improvement with number of synchronised SHNOs.

Fig.3b shows the synchronisation peak power at the same current values (white solid lines in Fig.2). As the total (integrated) microwave power should increase linearly with N for a mutually synchronized square array[30] we expect the peak power to increase as N^2. While this is observed for small N = 4–25 for all arrays, the peak power eventually levels off for larger N = 36–64. This roll off can be reproduced by introducing a small relative phase difference between individual constrictions or between individual chains. While this phase shift is negligible in small arrays, it will add up to a significant phase shift between the constrictions or chains farthest apart in the larger arrays. As the voltages are no longer added exactly in phase, the N^2 scaling will no longer hold. The dashed black line in Fig.3b is a calculation of the expected peak power using the measured resistance values for each array and the assumption that there is a chain-to-chain relative phase shift of 16°. The agreement is reasonably and indicates that the peak power would not increase substantially for 10×10 and larger arrays (see Methods, Estimated power spectral density for details).

In Fig.3c we show how the synchronisation current density (J_{Sync}; extracted from white dashed lines in Fig.2), depends on SHNO array dimensions. J_{Sync} is virtually independent of the number of SHNOs in the array as long as w and p stay the same. For the two arrays with w=120 nm, we can compare the impact of pitch and conclude that larger separation requires a slightly higher current density for mutual synchronisation. However, the overall trend is that J_{Sync} is rather independent on array dimensions at this level of detail.

The low linewidh of $\sim$60 kHz at an operating frequency of $\sim$10 GHz, leads to quality factors as high as $Q = f/\Delta f$ = 170,000. As the N^{-1} dependence of the linewidth does not show any sign of levelling off for higher N, mutual synchronisation of yet larger arrays can be pursued to further improve Q in the white noise regime. The very low white noise linewidth will greatly simplify the design of phase-locked loops[31] (PLLs) to further stabilize the microwave signal, as the PLL can be optimized for the slower $1/f$ noise still present in the synchronised state.

Prospect for neuromorphic computing

In addition to serving as highly coherent microwave sources, the two-dimensional SHNO arrays can be directly used for neuromorphic computing following an approach implemented using STNO vortex-oscillator chains[18]. As a proof-of-principle we have chosen a 4×4 SHNO array at an operating point where the four individual chains are mutually synchronised internally but do not synchronise with each other (Fig.4a). The four chains hence serve as the four neurons, N_{1-4}, which in our case interact in a predominantly nearest neighbor fashion. This is qualitatively different from the chains of vortex-oscillators, where all neurons interacted globally through their shared microwave current.[18] Fig.4c demonstrates that each chain remains in its internally synchronised state when subject to an injected microwave current at about twice its frequency[32] and that each neuron interacts individually with the injected current. Fig.4d finally shows the characteristic synchronisation map[18] of a 4-neuron oscillator network subject to two individually swept microwave frequencies f_A and f_B. Each colour represents one of the 20 different injection locked states as indicated to the right of the map. The network can hence distinguish and categorize 20 different input combinations of f_A and f_B.

Using synchronised chains as our neurons, instead of single constrictions, provides both higher coherence and higher output power, which simplifies the identification of the different synchronised states. It also demonstrates that mutual synchronisation within chains remains robust under external perturbations necessary for computing, which is an example of the versatility and robustness of the nano-constriction SHNOs. For completeness we point out that we could also generate 20-state synchronisation maps using four nano-constrictions in a 2×2 array, albeit with less signal quality (not shown).

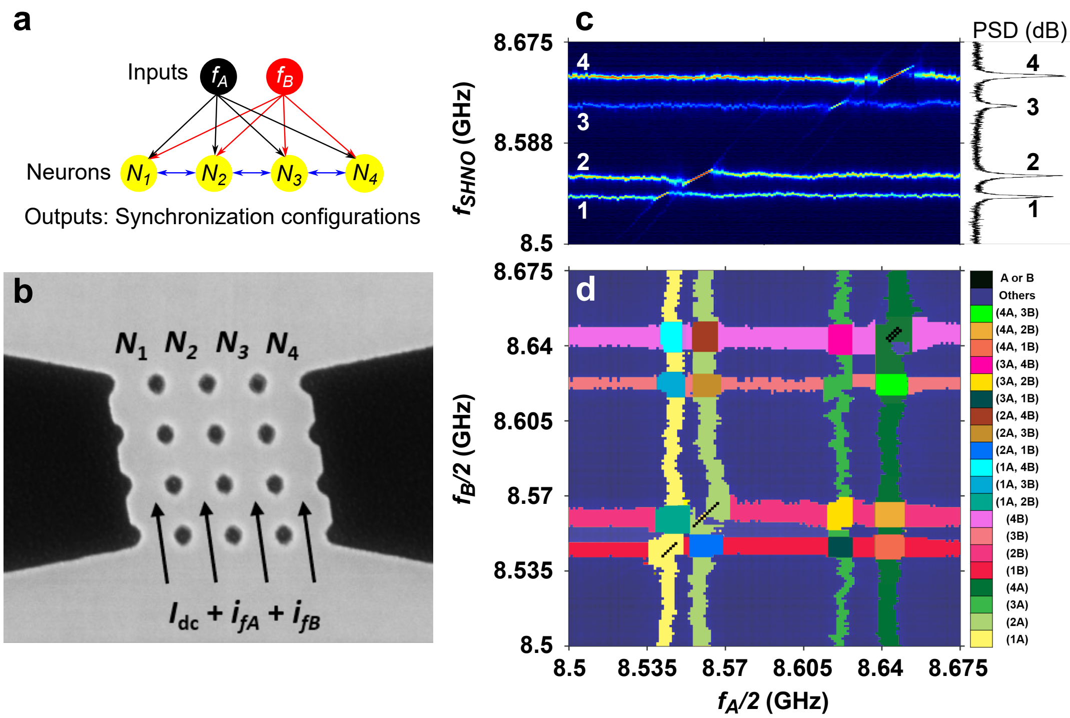

Figure 4: **Neuromorphic computing with a 4x4 SHNO array.** (**a**) Schematic of the network where the four neurons (N_{1-4}) interact only with their nearest neigbors while both input current (f_A and f_B) act globally on all four neurons. (**b**) SEM picture of the 4x4 array where the four synchronised chains act as neurons N_{1-4}, and two microwave currents with frequencies f_A and f_B are added to the drive current. (**c**) Injection locking to f_A of each synchronised chain. (**d**) synchronisation map of the network response when both f_A and f_B are swept individually. A total of 20 different injection locked responses can be observed. Each state is represented by its own colour in the list to the right of the map, where *e.g.* (1A, 2B) indicates that neuron 1 is locked to f_A and neuron 2 is locked to f_B, while the other neurons remain unlocked.

To train our network, we need a way to tune their individual frequencies. While one could imagine a layout that would allow for individual current tuning of different nano-constrictions or chains, this becomes increasingly complex for larger networks. A more useful approach would be direct voltage control of the magnetic properties in the nano-constriction region, such as the magnetic anisotropy and/or the damping[33,34] which could tune the SHNO frequency and possibly also turn them on/off at will. Particularly intriguing is the possibility of incorporating a non-volatile element in the voltage control of the magnitude and even sign of the spin orbit torque, as was recently shown[35,36], to allow for local storage of synaptic weights at each nano-constriction.

A wide range of recently suggested neuromorphic computing approaches are based on large two-dimensional oscillator network with local tuning. Vertex colour ing of graphs, which represents a class of combinatorial problems that are non-deterministic polynomial-time hard, can be addressed with oscillator networks.[37] Pattern matching using arrays of multilevel oscillator neurons has been suggested.[38,39] Auto-associative memory based on networks of STNOs and mechanical oscillators have been studied[12,40,41]. Oscillator networks with nearest-neighbor coupling instead of global coupling show particular potential for image segmentation and edge detection,[42,43] and can also be used as Ising machines for solving combinatorial optimisation problems.[44] The characteristic scale of image segmentation, *i.e.* whether fine or coarse grain details should be clustered together, is furthermore governed by the general nearest-neighbor coupling strength. As we can control this coupling both by the current and/or the external field, image segmentation at variable length scales should be possible using a single two-dimensional SHNO network with voltage controlled frequencies.

In comparison to one-dimensional STNO chains[18], two-dimensional SHNO arrays have a number of significant merits for neuromorphic computing. To perform classification or segmentation of bigger data sets, one must scale up the network as the maximum number of distinguishable classes or segments depend on the number of sufficiently interacting oscillators to provide a useful mix of partially synchronised states. Our SHNO arrays offer a proper scaling path, currently accommodating 100 partially synchronised SHNOs taking up an area of less than 1 μm^2; further down-scaling, using already demonstrated 20 nm SHNOs[45], will bring that number below 0.2 μm^2. The time required to reach a particular synchronised state is expected to scale inversely with the product of the operating frequency and the coupling strength. SHNO operation has been demonstrated at 24 GHz and the mutual locking range is of the order of 1 GHz,[21,25] both being about two orders of magnitude higher than the corresponding numbers for vortex STNOs[18,46]. The direct optical access may also enable optical inputs to the network.

To truly benefit from these improved characteristics, it will be important to increase the output power by other means than synchronisation. The best STNO output power has been demonstrated using magnetic tunnel junctions (MTJs).[47] MTJ based SHNO arrays should be possible to fabricate using *e.g.* W/CoFeB based tri–layers[21], where a W/CoFeB/MgO/CoFeB stack could define an MTJ on top of the auto-oscillating constriction region. By using MTJs over only part of a synchronised array, one may also circumvent the build up of a large phase shift between distant parts of the array.

Conclusion

In conclusion, we have fabricated two-dimensional SHNO arrays with up to N = 100 nano-constrictions and demonstrated robust mutual synchronisation in arrays with up to N = 64 constrictions. We find that the white noise linewidth scales inversely with the number of mutually synchronised constrictions and can reach below 60 kHz at frequencies of about 10 GHz, reaching Q values of 170,000. The $1/f$ noise is only marginally improved. We have also demonstrated how these two-dimensional arrays can produce the type of synchronisation maps recently used in neuromorphic computing. Our demonstration will enable the use of SHNO arrays in two-dimensional nano-oscillator networks for high-quality microwave signal generation and neuromorphic computing on very large data sets.

Methods

Sample fabrication. To fabricate SHNO arrays, a tri-layer of $Ni_{80}Fe_{20}$(3nm)/Hf(0.5nm)/Pt(5nm) was deposited at room temperature on high resistivity silicon substrate (10 kΩ.cm). The native oxide layer on the substrate was removed by plasma cleaning before the deposition process. An ultra high vacuum magnetron sputtering machine was used while the Ar pressure was kept at 3 mTorr during the deposition. The sample was covered by 37nm of Hydrogen silsesquioxane (HSQ) electron beam resist and SHNO arrays were written in HSQ by a Raith EBPG 5200 electron beam lithography machine operating at 100 kV. The patterns were then transferred to the tri–layer by ion beam milling process at 30° ion incident angle with respect to the film normal to minimize sidewall redepositions. SHNO arrays were defined with different constriction widths (w = 50, 80, and 120 nm) and SHNOs center to center distance as pitch size (p = 100, 140, 200, 300 nm). Because the curvature of the nano constriction is rather elliptical arc, for the larger p values, the shape of the holes defined into the tri–layer is more elliptical. However, for smaller p values, the holes look more circular. The curvatures of the nano constrictions in all arrays with different ws and ps are identical. To define the top coplanar waveguide (CPW) contact for dc and microwave measurements, optical lithography was performed followed by HSQ removal only at contact areas in diluted buffered Hydrofluoric acid. Finally, a 1 μm thick layer of Cu(980nm)/Pt(20nm) was deposited, and CPWs were obtained after resist removal by the lift-off process.

Microwave characterisation We used a custom-built probe station where the stage can rotate the sample holder between the poles of an electromagnet to apply an out-of-plane magnetic field to the sample. The in-plane and out-of-plane angles of the sample were fixed at 30° and 76°, respectively while the magnetic field was set to $\mu_0 H$= 0.68 T for all measurements. A direct current was applied through the dc port of a bias-T to excited auto oscillation in SHNO array while emitted microwave signal from array was picked up by the high frequency port of bias-T and was sent to a low noise amplifier (LNA) in 4-10 GHz range before it was recorded by a high frequency spectrum analyzer (SA). The recorded spectra were then corrected to correspond to the power emitted by the device, taking into account the amplifier gain, the losses from the radio frequency (rf) components and cables, and the impedance mismatch between the device and the 50 Ω measurement line and load. The auto-oscillation linewidth and peakpower were extracted by fitting a single symmetric Lorentzian function. To perform the neuromorphic computing demonstration, we used a microwave power combiner connected to a microwave circulator to inject two microwave signals into the SHNO arrays. The injected power for the two signals f_{A} and f_{B} was limited to –2 dBm to avoid any damage to the LNA and the SA. f_{A} and f_{B} were chosen to be close to $2f_{\mathrm{SHNO}}$, *i.e.* we injection lock on the second harmonic.

Estimated power spectral density We consider the power delivered by the array of $K \times M = N$ oscillators to the load R_l, taking into account the finite resistance of the mesa R_m. For the perfectly synchronised state, without any phase shift between oscillators, the power reads as [30]:

$$P_N = \left[\frac{KMI_{dc}\Delta R_{ac}}{KR_c + M(R_l + R_m)}\right]^2 R_l, \tag{1}$$

where M defines the quantity of parallel branches with K serial oscillators in each of them and, thus, for our case $K = M = 2, 4, 5, 6, 8$. $R_l = 50\Omega$ - load resistance, $R_m = 200\Omega$ is the resistance of the sample outside the array region (mesa), $R_c = 80\Omega$ - the resistance of each nano-constriction, I_{dc} - dc current applied to each oscillator and R_{ac} is the alternate resistance created by the magnetisation precession through AMR, which we assume as a fitting parameter.

Please note, that the above expression results in the proportionality of the delivered power to the total number of oscillators N for the square arrays, when $K = M$. Since the measured power deviates from such a scaling, we we allow for a phase shift ϕ between neighboring chains. In this case, assuming the Lorentzian shape of the PSD with the linewidth Δf defined by full width at half maximum (FWHM), one can write the maximum value of the PSD:

$$\mathrm{PSD}_{max} = \frac{2}{\pi\Delta f}\left[\frac{KI_{dc}\Delta R_{ac}}{KR_c + M(R_l + R_m)}\sum_{j=0}^{M-1}\cos j\phi\right]^2 R_l^2, \tag{2}$$

which is shown by a dashed line on Fig. 3b with the fitted value $\phi = 16.4°$. Please note, that in the synchronised state the linewidth Δf should be inversely proportional to the total power of auto-oscillations, i.e. to the total number N, and does not depend on the phase shift ϕ [48].

Micro–BLS characterisation The magneto-optical measurements were performed using room temperature micro-focused BLS measurements. Spatially resolved maps of the magnetisation dynamics are obtained by focusing a polarized monochromatic 532 nm single frequency laser (solid state diode-pumped) using a high numerical aperture (NA=0.75) dark-field objective, which yields a diffraction limited resolution of 360 nm. The scattered light from the sample surface is then analysed by a high-contrast six-pass Tandem Fabry-Perot interferometer TFP-1 (JRS Scientific Instruments). The obtained BLS intensity is proportional to the square of the amplitude of the magnetisation dynamics at the corresponding frequency.

Data Availability Statement The data that support the plots within this paper and other findings of this study are available from the corresponding author upon reasonable request.

Code availability statement The MATLAB codes used in this study are available from the corresponding author upon reasonable request.

1. Grollier, J., Querlioz, D. & Stiles, M. D. Spintronic nanodevices for bioinspired computing. *Proceedings of the IEEE* **104**, 2024–2039 (2016).

2. Pufall, M. R. *et al.* Physical implementation of coherently coupled oscillator networks. *IEEE Journal on Exploratory Solid-State Computational Devices and Circuits* **1**, 76–84 (2015).

3. Locatelli, N., Cros, V. & Grollier, J. Spin-torque building blocks. *Nature Materials* **13**, 11 (2014).

4. Xu, X. *et al.* Scaling for edge inference of deep neural networks. *Nature Electronics* **1**, 216 (2018).

5. Buzsaki, G. *Rhythms of the Brain* (Oxford University Press, 2006).

6. Kumar, S., Strachan, J. P. & Williams, R. S. Chaotic dynamics in nanoscale nbo 2 mott memristors for analogue computing. *Nature* **548**, 318 (2017).

7. Ignatov, M., Ziegler, M., Hansen, M. & Kohlstedt, H. Memristive stochastic plasticity enables mimicking of neural synchrony: Memristive circuit emulates an optical illusion. *Science Advances* **3**, e1700849 (2017).

8. Segall, K. *et al.* Synchronization dynamics on the picosecond time scale in coupled josephson junction neurons. *Physical Review E* **95**, 032220 (2017).

9. Galin, M. A. *et al.* Synchronization of large josephson-junction arrays by traveling electromagnetic waves. *Physical Review Applied* **9**, 054032 (2018).

10. Inagaki, T. *et al.* A coherent ising machine for 2000-node optimization problems. *Science* **354**, 603 (2016).

11. McMahon, P. L. *et al.* A fully programmable 100-spin coherent ising machine with all-to-all connections. *Science* **354**, 614–617 (2016).

12. Fang, Y., Yashin, V. V., Levitan, S. P. & Balazs, A. C. Pattern recognition with "materials that compute". *Science Advances* **2**, e1601114 (2016).

13. Shim, S.-B., Imboden, M. & Mohanty, P. Synchronized oscillation in coupled nanomechanical oscillators. *Science* **316**, 95–99 (2007).

14. Csaba, G. & Porod, W. Computational study of spin-torque oscillator interactions for non-boolean computing applications. *IEEE Transactions on Magnetics* **49**, 4447–4451 (2013).

15. Yogendra, K., Fan, D., Jung, B. & Roy, K. Magnetic pattern recognition using injection-locked spin-torque nano-oscillators. *IEEE Transactions on Electron Devices* **63**, 1674–1680 (2016).

16. Chen, T. *et al.* Spin-torque and spin-hall nano-oscillators. *Proceedings of the IEEE* **104**, 1919–1945 (2016).

17. Rippard, W. H., Pufall, M. R., Kaka, S., Silva, T. J. & Russek, S. E. Current-driven microwave dynamics in magnetic point contacts as a function of applied field angle. *Phys. Rev. B* **70**, 100406 (2004).

18. Romera, M. *et al.* Vowel recognition with four coupled spin-torque nano-oscillators. *Nature* **563**, 230–234 (2018).

19. Demidov, V. E. *et al.* Magnetic nano-oscillator driven by pure spin current. *Nature Mater.* **11**, 1028–1031 (2012).

20. Ranjbar, M. CoFeB-Based Spin Hall Nano-Oscillators. *Ieee Magnetics Letters* **5**, 1–4 (2014).

21. Zahedinejad, M. *et al.* Cmos compatible w/cofeb/mgo spin hall nano-oscillators with wide frequency tunability. *Applied Physics Letters* **112**, 132404 (2018).

22. Demidov, V. E. *et al.* Magnetic nano-oscillator driven by pure spin current. *Nature materials* **11**, 1028 (2012).

23. Demidov, V. E., Urazhdin, S., Zholud, A., Sadovnikov, A. V. & Demokritov, S. O. Nanoconstriction-based spin-Hall nano-oscillator. *Appl. Phys. Lett.* **105**, 172410 (2014).

24. Fulara, H. *et al.* Spin-orbit torque–driven propagating spin waves. *Science Advances* **5**, eaax8467 (2019).

25. Awad, A. *et al.* Long-range mutual synchronization of spin hall nano-oscillators. *Nature Physics* **13**, 292 (2017).

26. Kim, J.-V., Tiberkevich, V. & Slavin, A. Generation Linewidth of an Auto-Oscillator with a Nonlinear Frequency Shift: Spin-Torque Nano-Oscillator. *Physical Review Letters* **100**, 1–4 (2008).

27. Mazraati, H., Zahedinejad, M. & Åkerman, J. Improving the magnetodynamical properties of nife/pt bilayers through hf dusting. *Applied Physics Letters* **113**, 092401 (2018).

28. Dvornik, M., Awad, A. A. & Åkerman, J. Origin of magnetization auto-oscillations in constriction-based spin hall nano-oscillators. *Physical Review Applied* **9**, 014017 (2018).

29. Keller, M. W., Pufall, M. R., Rippard, W. H. & Silva, T. J. Nonwhite frequency noise in spin torque oscillators and its effect on spectral linewidth. *Physical Review B* **82**, 054416 (2010).

30. Georges, B., Grollier, J., Cros, V. & Fert, A. Impact of the electrical connection of spin transfer nano-oscillators on their synchronization: an analytical study. *Appl. Phys. Lett.* **92**, 232504 (2008).

31. Tamaru, S., Kubota, H., Yakushiji, K., Yuasa, S. & Fukushima, A. Extremely coherent microwave emission from spin torque oscillator stabilized by phase locked loop. *Scientific Reports* **5**, 18134 (2015).

32. Demidov, V. *et al.* Synchronization of spin hall nano-oscillators to external microwave signals. *Nature communications* **5**, 3179 (2014).

33. Matsukura, F., Tokura, Y. & Ohno, H. Control of magnetism by electric fields. *Nature nanotechnology* **10**, 209 (2015).

34. Liu, R., Chen, L., Urazhdin, S., Du, Y. *et al.* Controlling the spectral characteristics of a spin-current auto-oscillator with an electric field. *Physical Review Applied* **8**, 021001 (2017).

35. Mishra, R. *et al.* Electric-field control of spin accumulation direction for spin-orbit torques. *Nature communications* **10**, 248 (2019).

36. Mishra, R., Kumar, D. & Yang, H. Oxygen-migration-based spintronic device emulating a biological synapse. *Physical Review Applied* **11**, 054065 (2019).

37. Parihar, A., Shukla, N., Jerry, M., Datta, S. & Raychowdhury, A. Vertex coloring of graphs via phase dynamics of coupled oscillatory networks. *Scientific reports* **7**, 911 (2017).

38. Velichko, A., Belyaev, M. & Boriskov, P. A model of an oscillatory neural network with multilevel neurons for pattern recognition and computing. *Electronics* **8**, 75 (2019).

39. Zhang, T., Haider, M., Massoud, Y. & Alexander, J. An oscillatory neural network based local processing unit for pattern recognition applications. *Electronics* **8**, 64 (2019).

40. Kumar, A. & Mohanty, P. Autoassociative memory and pattern recognition in micromechanical oscillator network. *Scientific reports* **7**, 411 (2017).

41. Nikonov, D. E. *et al.* Coupled-oscillator associative memory array operation for pattern recognition. *IEEE Journal on Exploratory Solid-State Computational Devices and Circuits* **1**, 85–93 (2015).

42. Fang, Y., Yashin, V. V., Jennings, B. B., Chiarulli, D. M. & Levitan, S. P. A simplified phase model for simulation of oscillator-based computing systems. *ACM Journal on Emerging Technologies in Computing Systems (JETC)* **13**, 14 (2017).

43. Novikov, A. & Benderskaya, E. Oscillatory network based on kuramoto model for image segmentation. In *International Conference on Parallel Computing Technologies*, 210–221 (Springer, 2015).

44. Wang, T., Wu, L. & Roychowdhury, J. New computational results and hardware prototypes for oscillator-based ising machines. In *Proceedings of the 56th Annual Design Automation Conference 2019*, 239 (ACM, 2019).

45. Dürrenfeld, P., Awad, A. A., Houshang, A., Dumas, R. K. & Åkerman, J. A 20 nm spin hall nano-oscillator. *Nanoscale* **9**, 1285–1291 (2017).

46. Lebrun, R. *et al.* Mutual synchronization of spin torque nano-oscillators through a long-range and tunable electrical coupling scheme. *Nature Communications* **8**, 15825 (2017).

47. Tsunegi, S. *et al.* Scaling up electrically synchronized spin torque oscillator networks. *Scientific Reports* **8**, 13475 (2018).

48. Wiesenfeld, K., Benz, S. P. & Booi, P. Phase-locked oscillator optimization for arrays of josephson junctions. *Journal of Applied Physics* **76**, 3835–3846 (1994).

Acknowledgements This work was partially supported by the European Research Council (ERC) under the European Union's Seventh Framework Programme (FP/2007-2013 ERC Grant No. 307144 "MUSTANG") and Horizon 2020 research and innovation programme (ERC Advanced Grant No. 835068 "TOPSPIN"). This work was also partially supported by the Swedish Research Council (VR) and the Knut and Alice Wallenberg Foundation.

Competing Interests The authors declare that they have no competing financial interests.

Authors contributions M.Z. designed and fabricated the devices, and carried out most of the electrical measurements and analysis of their microwave signal properties. A.A. and S. M. carried out all Brillouin Light Scattering measurements and analysis as well as the neuromorphic demonstration. R.K. and M.D. assisted with theoretical support and analysis. H.F. and H.M. assisted with microwave measurements and analysis. All authors contributed to the data analysis and co-wrote the manuscript.

Correspondence Correspondence and requests for materials should be addressed to J. Åkerman (email: johan.akerman@physics.gu.se).